A role for the cortex in sleep-wake regulation

Lukas B. Krone[1,2], Tomoko Yamagata[2,3], Cristina Blanco-Duque[1,2],
Mathilde C. C. Guillaumin[2,3], Martin C. Kahn[1,2], Colin J. Akerman[4],
Anna Hoerder-Suabedissen[1], Zoltán Molnár[1], Vladyslav V. Vyazovskiy[1,2]

Affiliations

[1] Department of Physiology, Anatomy and Genetics, University of Oxford, UK

[2] Sleep and Circadian Neuroscience Institute, University of Oxford, UK

[3]Nuffield Department of Clinical Neurosciences, University of Oxford, UK

[4] Department of Pharmacology, University of Oxford, UK

Key words: sleep homeostasis, cortex, layer 5, EEG, slow-wave activity, sleep, SNAP25

Corresponding authors

Vladyslav V. Vyazovskiy
Department of Physiology, Anatomy and Genetics,
Sleep and Circadian Neuroscience Institute (SCNi),
Dunn School of Pathology, South Parks Road, Oxford, OX1 3RE
Phone: +44 (0) 1865 618676
E-mail: vladyslav.vyazovskiy@dpag.ox.ac.uk

Zoltán Molnár
Department of Physiology, Anatomy and Genetics,
Sherrington Building, Sherrington Road, Oxford, OX1 3PT
Phone: +44 (0) 1865 610875
E-mail: zoltan.molnar@dpag.ox.ac.uk

Abstract

The cortex and subcortical circuitry are thought to play distinct roles in the generation of sleep oscillations and global control of vigilance states. Here we show in mice that cell-specific ablation of the key t-SNARE protein SNAP25 in a subset of cortical layer 5 pyramidal and dentate gyrus granule cells results in a marked increase in wakefulness accompanied by a reduced rebound of EEG slow-wave activity after sleep deprivation. The data suggest an important role of the cortex in both global state control and sleep homeostasis.

Main text

Sleep is not an optional behaviour, and its duration, timing and architecture are under strict regulation. Early studies based on neurological case reports, transections and electrical stimulation suggested that global state transitions are mediated via a distributed circuitry across the brainstem, the hypothalamus and the basal forebrain[1,2]. Recent studies using selective targeting of subcortical neuronal populations based on their gene expression or connectivity patterns, have highlighted a growing complexity within the sleep-wake promoting circuitry, with distinct neuronal subtypes responsible for specific aspects of wakefulness and sleep[3,4]. While sleep-wake states are defined by the occurrence of neocortical and hippocampal oscillations[5], the role of cortical structures in global vigilance state control has received considerably less attention.

Previous work suggests that cortical oscillations and neuronal firing patterns mirror another major process in sleep regulation, so called sleep homeostasis[6,7]. Sleep homeostasis refers to the capacity to adapt the duration and intensity of sleep to the duration of preceding wakefulness[6]. Electroencephalogram (EEG) slow-wave activity (SWA, EEG spectral power between 0.5-4 Hz) represents a reliable marker of sleep-wake history[6] and has been proposed to underlie many functions of sleep, such as the need for cellular maintenance[8] or synaptic plasticity[9]. Studies suggest that cortical SWA is regulated in a local, use-dependent manner[10,11] supporting the view that sleep emerges within cortical networks as a result of a local accumulation of products of metabolism, such as adenosine[12]. However, the capacity to produce slow waves does not automatically imply a role for the cortex in sleep or sleep homeostasis, either on a local or global level. Indeed, slow waves can occur under anaesthesia, in isolated cortical slabs or even *ex vivo*[13–16]. Therefore, it remains unclear whether the neocortex is merely responsible for sustaining this default type of oscillation, or whether it contributes actively to sleep homeostasis and global sleep-wake control.

In this study we set out to address whether cortical structures have a function in generating or sensing local homeostatic sleep need and thereby influence global sleep-wake dynamics. We focused on pyramidal neurons within layer 5 of cortex, which possess a set of potentially relevant properties including high dendritic spine density and axonal arborisation[17] and high sensitivity to adenosine[18]. Furthermore, several studies suggest that layer 5 pyramidal neurons, and specifically slow intrinsically bursting neurons unique to this layer[19], play a key role in the initiation and propagation of cortical slow waves[19–22].

We first performed laminar local field potential (LFP) and multiunit (MUA) recordings from the primary motor cortex, concomitantly with EEG and electromyography (EMG) monitoring in male adult mice during 24 h baseline, as well as during and after 6 h of sleep deprivation (Figure 1A-D). As expected, the laminar profile of LFPs and MUAs revealed generally activated patterns during waking and rapid eye movement (REM) sleep as well as an occurrence of depth positive LFP slow waves associated with a generalised suppression of spiking activity observed across cortical layers during non-rapid eye movement (NREM) (Figure 1C)[23,24]. Neurons were generally more active in the deep layers of the motor cortex, especially in layer 5 (Figure 1C,E), as was observed in previous studies[22]. Consistent with the notion of an active role of layer 5 in shaping sleep oscillations[17,20,21], we also found that neurons in layer 5 tended to initiate spiking upon the onset of population ON periods (Figure 1E,F,G). The leading role of layer 5 in OFF-ON dynamics was indicated by a stronger initial surge of firing rates at OFF-ON transitions (Figure 1F) and a shorter latency to the first spike during ON periods, even when the total number of spikes in layer 5 was precisely matched with layer 2/3 (Figure 1G).

To induce a cortex-wide reduction in the output from layer 5 pyramidal neurons, we generated a transgenic mouse line, in which a subpopulation (~ 15-30 %) of pyramidal cells in layer 5 of the neocortex lacked the key t-SNARE protein SNAP25 (Rbp4-Cre;Ai14;Snap25$^{fl/fl}$)[25]. While Rbp4-Cre is known as a pan layer 5 driver line[26], it additionally presents a strong Cre-expression in hippocampal dentate gyrus, but was only sparsely expressed in the hypothalamus, typically considered a major brain area involved in sleep-wake state transitions (Suppl. Figure 1). Selective targeting of Rbp4-Cre to layer 5 was confirmed using DAPI histology to define cortical layers and a tdTomato reporter to identify Cre-expressing cells (Figure 1H and Suppl. Figure 2). Cre-dependent excision of exon 5a/5b leads to reduced length gene transcript and non-detectable levels of SNAP25 protein in Cre-positive neurons[25]. As well known, ablation of SNAP25 virtually abolishes calcium-evoked neurotransmitter release from the respective neurons[25,27], which renders the cells carrying the mutation functionally silenced.

Transgenic animals (Rbp4-Cre;Ai14;Snap25$^{fl/fl}$) did not show obvious physical, neurological or behavioural abnormalities but their body weight was lower compared to controls (CTR: 23.4g, HOM: 20.9g, $t(13)=2.87$, $p=0.013$) as reported previously[25]. The electrophysiological signals revealed typical signatures of wakefulness and sleep states. Importantly, ablation of SNAP25 did not result in significant changes in absolute EEG power spectra during NREM sleep or in the occurrence of slow waves (Figure 1I), although a leftward

shift of the theta-peak frequency was observed during REM sleep (Suppl. Figure 3). This result is in line with the observation that Rbp4 expression is not restricted to the layer 5 of the neocortex, but is also present in granule cells of the hippocampal dentate gyrus[25], which is involved in generating theta activity during REM sleep[28,29].

While baseline differences in sleep oscillations between the genotypes were modest, the overall daily sleep-wake profile of cortical SNAP25-ablated animals showed marked differences (Figure 2A). Control animals showed generally a higher amount of waking during the dark period as compared to the light phase, but short bouts of sleep were common, as typically observed in C57BL6 mice (Figure 2B)[30]. In contrast, upon dark onset cortical SNAP25-ablated animals showed unusually long wake bouts that often persisted for at least several hours (Figure 2B,E). On average, over 24h these animals spent 13.83±0.39 h awake, which is 31 % more than control animals (10.57±0.42 h, $t(13)=5.55$, $p<0.001$, two-tailed t-test for independent samples), and the amount of sleep was proportionally decreased (Figure 2C). The differences between genotypes were primarily evident in the dark period (Figure 2D and Suppl. Figure 4). The increased capacity to engage in prolonged waking periods in cortical SNAP25-ablated animals may suggest either a slower accumulation of sleep pressure during waking or a deficiency in translating the accumulated sleep need into an adequate homeostatic response during subsequent sleep. To investigate these possibilities, we next detected all consolidated wake bouts longer than 15 min across 24 h and compared the levels of EEG SWA during NREM sleep for 15 min time windows preceding and following individual wake episodes. As expected[31], a positive correlation was observed in both genotypes, whereby longer spontaneous wake periods were followed by proportionally higher levels of SWA during NREM sleep (Figure 2F). However, the increase of SWA relative to the duration of wake episodes was significantly smaller in cortical SNAP25-ablated animals compared to controls (Figure 2F). This finding indicates that ablation of SNAP25 in the neocortex and the hippocampus affects the relationship between sleep-wake history and the homeostatic response of SWA.

An established approach to investigate the dynamics of sleep homeostasis is sleep deprivation, which is typically performed starting at light onset, when mice in laboratory conditions usually sleep[7,30]. Sleep deprivation was successfully imposed in both genotypes, as only a minimal amount of time (SNAP25-ablated: 1.84±0.75 %, controls: 1.39±0.32 %) was spent asleep during the 6-h interval when the mice were kept awake by providing novel objects continuously. Typically, sleep deprivation leads to a subsequent increase in NREM sleep, SWA, and sleep amount. However, we observed a striking difference in this homeostatic

rebound between genotypes (Figure 3A-G). This manifested in a marked attenuation of the initial increase of EEG SWA during NREM sleep after sleep deprivation in cortical SNAP25-ablated animals (relative SWA in SNAP25-ablated: 136.77±3.98 %, controls: 180.57±5.13 %, first 30 min post SD, $t(11)=6.78$, $p<0.001$, two-tailed t-test for independent samples, Figure 3B), which was especially pronounced in frequencies between 1.5 and 3.75 Hz (Figure 3C). Interestingly, the difference was restricted to the frontal EEG but was not found in the occipital derivation, consistent with the idea that homeostatic elevation of SWA is a predominantly frontal phenomenon (Suppl. Figure 5)[32]. Since consolidation and fragmentation of sleep are sensitive behavioural measures of homeostatic sleep pressure[33], we next analysed sleep architecture in greater detail. Both genotypes showed an increase in NREM sleep amount during the recovery period (Figure 3D), and the duration of NREM sleep episodes was initially longer than during baseline (Figure 3E). However, during the dark period following SD cortical SNAP25-ablated animals still presented markedly prolonged episodes of wakefulness and an overall reduced amount of sleep compared to controls, as if sleep pressure were low (Figure 3F,G). Taken together, the data suggest that preceding sleep-wake history is not effectively encoded in cortical SNAP25-ablated mice.

In summary, our study suggests an important role for the cortex not only in the dynamics of local network oscillations, but also in sleep homeostasis and the global control of sleep-wake states. This finding supports the idea that brain structures fundamentally involved in sleep regulation extend far beyond the traditionally considered subcortical circuitry[4,12,34]. Whilst it remains open where and in what form the need to sleep is encoded in mammals[35], our data leave no doubt that cortical structures play an important role. One possibility is that homeostatic sleep need is generated locally in the cortex itself in an activity-dependent fashion, as it has been earlier proposed[8,12]. Alternatively, cortical structures may be the key site which integrates the information about levels of sleep need, which accumulate during wakefulness elsewhere. At the molecular and cellular levels, signals reflecting wake-dependent increase in sleep need, conserved both in mammalian and non-mammalian species, may represent changes in synaptic phosphoproteome[36,37], endoplasmic reticulum stress[38], or redox homeostasis[39]. Yet, such changes may and indeed likely occur across brain-wide distributed networks, and this must be translated into an adequate homeostatic response, reflected in an occurrence of intense sleep, characterised by high cortical SWA. We hypothesise that the wide connectivity of layer 5 pyramidal neurons to other parts of cortex, thalamus, and potentially sleep-wake regulating nuclei in the brainstem[26] places this neuronal population in an ideal position not only to

generate SWA, but also to sense and integrate the signals related to sleep need, and ultimately broadcast the information to the subcortical circuitry responsible for sleep-wake switching[3].

While the Rbp4-Cre mouse line is widely used as a driver line specific for layer 5 pyramidal neurons, it is important to highlight that the genetic manipulation used in this study targeted not only a subpopulation of layer 5 projection neurons of the neocortex, but also the dentate gyrus of the hippocampus, which possibly has a unique and distinct contribution to the striking sleep phenotype we describe here. It can be speculated that altered neurotransmission in neocortical layer 5 could underpin the deficit in the homeostatic SWA response after prolonged wakefulness. On the other hand, the hippocampus, given its critical place in the brain-wide circuitry involved in memory and temporal processing[40], could have a so far unrecognised role in encoding time spent awake or asleep, i.e. sleep-wake history.

We cannot entirely exclude the role of developmental compensation or a possibility that a small proportion of cells in other brain regions were functionally silenced in this mouse line. However, the most parsimonious explanation for the profound alterations in sleep architecture and sleep homeostasis we observed is that cortical structures play a fundamental role in sleep regulation. We posit that cortex is not merely changing its activity depending on how much time has passed awake or asleep, but that it actively contributes to the flipping of the sleep-wake switch.

Methods

Animals

EEG/EMG implants were performed in 7 wild type C57BL/6 mice (WT, surgery weight 29.5±0.8 g, age at day of baseline recording 125±8 days), 9 Rbp4-Cre;Ai14;Snap25$^{fl/fl}$ mice (HOM, surgery weight 20.9±0.6 g, age at day of baseline recording 86±6 days) and 6 Cre-negative littermates (CTR, surgery weight 23.4±0.6 g, age at day of baseline recording 78±5 days) under isoflurane anaesthesia as described previously[41]. For technical reasons, the EEG datasets from 1 HOM and 1 CTR could only be used for vigilance state analysis but had to be excluded from the analyses of EEG spectra. We recorded laminar LFP and MUA signals in WT mice across cortical layers in primary motor cortex (+ 1.1 mm AP (anterior), - 1.75 mm ML (left), tilt -15° (left)) using 16-channel silicon probes (NeuroNexus Technologies Inc., Ann Arbor, MI, USA; model: A1x16-3mm-100-703-Z16) with a spacing of 100 µm between individual channels. In a subset of HOM and CTR animals, laminar recordings were also obtained but were not included in the manuscript due to the low number of animals, which prevent us from reaching any solid conclusions.

Rbp4-Cre;Ai14;Snap25$^{fl/fl}$ is a triple transgenic mouse line, which was designed as a model for functional silencing of cortical layer 5 pyramidal and dentate gyrus granule cells. Snap25$^{fl/fl}$ is a transgene, with lox-P sites flanking the alternatively spliced exons 5a and 5b of the t-SNARE (target membrane soluble N-ethylmaleimide-sensitive factor attachment protein (SNAP) receptor) gene *Snap25* leading to virtually complete absence of SNAP25 and cessation of Ca^{2+}-dependent evoked synaptic vesicle release[25].

All mice were housed individually in open cages before surgery and in individually ventilated cages during a recovery period of about one week after surgery. For sleep recordings, mice were allowed at least three days of acclimatization to custom-made individual plexiglas cages (20.3 x 32 x 35 cm), which were placed in sound-attenuated and light-controlled Faraday chambers (Campden Instruments, Loughborough, UK). Animals were allowed free access to food pellets and water at all times and underwent daily health inspection. A 12 h:12 h light-dark cycle (lights on at 9 am, light levels 120–180 lux) was implemented and temperature maintained at around 22 ± 2°C.

Experimental procedures

After habituation to the recording setup of at least 3 days, a 24 h period of continuous recordings starting at light onset was performed on a designated baseline day. On the following day, all animals were sleep deprived for 6h starting at light onset by exposure to novel objects under continuous observation by experimenters. When mice stopped exploring the provided objects, new objects were placed into the cage to stimulate exploratory wakefulness.

Data acquisition, data processing, and sleep scoring

Electrophysiological in vivo recordings. Data was acquired using the 128 Channel Neurophysiology Recording System (Tucker-Davis Technologies Inc., Alachua, FL, USA) and the electrophysiological recording software Synapse (Tucker-Davis Technologies Inc., Alachua, FL, USA) and saved on a local computer. EEG and EMG signals were continuously recorded, filtered between 0.1 - 100 Hz, and stored at a sampling rate of 305 Hz. Extracellular neuronal activity was continuously recorded at a sampling rate of 25 kHz and filtered between 300 Hz - 5 kHz. Whenever the recorded voltage in an individual laminar channel crossed a manually set threshold indicating putative neuronal firing (at least 2 standard deviations above noise level), 46 samples around the event (0.48 ms before, 1.36 ms after) were stored. Concomitantly with the spike acquisition, LFPs were continuously recorded from the same electrodes and processed with the abovementioned settings for EEG signals.

Offline signal processing. EEG, EMG, and LFP signals were resampled at a sampling rate of 256 Hz and converted into text files with custom-made code in Matlab (The MathWorks Inc, Natick, Massachusetts, USA, version v2017a). The open source software Neurotraces was used for a subsequent conversion into the European Data Format (EDF). Spike wave forms were further processed using a custom-made Matlab script and events with artefactual wave forms were excluded from further analysis of neuronal activity.

Scoring of vigilance states and recording artefacts. The software Sleep Sign for Animals (SleepSign Kissei Comtec Co., Ltd., Nagano, Japan) was used for sleep scoring. EEG, EMG, and LFP recordings were partitioned into epochs of 4 seconds length. Vigilance states were

assigned manually to each recording epoch based on visual inspection of the frontal and occipital EEG derivations in conjunction with the EMG. For two animals with defective EEG reference, a fronto-occipital EEG derivation was used for sleep scoring. Epochs with recording artefacts due to gross movements, chewing or external electrostatic noise were assigned to the respective vigilance state but not included in the electrophysiological analysis. Overall 18.8±3.5 % of wake, 0.7±0.4 % of NREM, and 0.9±0.4 % of REM epochs contained artefactual EEG signals with no significant difference between genotypes. EEG and LFP power spectra were computed using a fast Fourier transform routine (Hanning window) with a 0.25Hz resolution and exported in the frequency range between 0 and 30 Hz for spectral analysis.

Statistical analysis

Data were analysed using MATLAB (version R2017b; The MathWorks Inc, Natick, Massachusetts, USA) and IBM SPSS Statistics for Windows, version 25.0 (IBM Corp., Armonk, N.Y., USA). Reported averages are mean±s.e.m. For analysis of repeated measures with more than 20 time or frequency bins (i.e. time courses of firing rates, latency to first spike for different spike numbers, and comparison of EEG power spectra), we performed unpaired t-tests for each individual time or frequency bin. Bins for which the resulting p-value was below 0.05 are highlighted with stars to indicate areas of interest bearing in mind that no correction for multiple comparisons was applied. EEG power spectra of individual animals were log-transformed before hypothesis testing. For comparison of time course data with less than 20 bins (i.e. time course of SWA after sleep deprivation or time course of time spent in NREM sleep), mixed ANOVAs with the within-subject factor 'time interval' and the between-subject factor 'genotype' or repeated-measure ANOVAs with the within-subject factors 'time-interval' and 'experimental condition' were applied and post-hoc comparisons were made using two-tailed unpaired or paired t-tests on individual time bins. Greenhouse-Geisser correction was used when the assumption of sphericity was violated (Mauchly's test of sphericity, p-value <0.05). For the comparison of vigilance state duration between genotypes, we performed two-tailed t-tests or alternatively Mann-Whitney U tests if the assumption of normality was violated. The NREM bout duration was compared between genotypes and time points using a mixed ANOVA with the within-subject factor 'experimental condition' and the between-subject factor 'genotype'. Post-hoc comparisons were performed using two-tailed paired t-tests to compare time points for each genotype and using two-tailed unpaired t-tests to compare genotypes at each time point. In all figures, significance levels are indicated with stars: '*' for

0.05 > p > 0.01; '**' for 0.01 > p > 0.001; '***' for 0.001 > p. Panels presenting grouped data of durations spent in specific vigilance states show group mean (red line), 95% confidence interval (pink box), and one standard deviation (blue box) with individual data points overlaid and were generated using the MATLAB function notBoxPlot (Rob Campbell (2019). notBoxPlot (https://www.github.com/raacampbell/notBoxPlot), GitHub. Retrieved June 15, 2019).

Criteria for analysis of vigilance state episodes and OFF periods

For analyses of mean and maximum duration of sustained wake episodes (Figure 2E), we included wake episodes, which were at least 1-min long allowing brief intrusions of sleep of 1 min or less. For the analysis of mean duration of NREM episodes, we included NREM episodes, which were at least 1-min long allowing brief intrusions of REM sleep or brief awakenings of 1 min or less (Figure 3E). To investigate the change in NREM SWA across prolonged wake episodes, we included consolidated periods of waking lasting at least 15 min, whereby short episodes of sleep <1 min were not considered as interruptions. We then performed analyses of NREM sleep SWA in the 15-min time window immediately preceding and following prolonged (>15 min) wake episodes if both time windows included at least 10 min of artefact-free NREM sleep and no more than 3 min of wakefulness (Figure 2F).

Population OFF periods were defined as periods of total neuronal silence across all electrodes which lasted at least 50 ms and no more than 4000 ms. Subsequently, the top 20% longest OFF periods were included for final analyses (Fig 1F,G). The latency to the first spike after the population OFF-ON transition was calculated separately for MUA recorded in layers 2/3 and layer 5. Only ON periods with at least 1 spike in each of the layers occurring within the first 200 ms were included in this analysis (Figure 1G).

Histological assessment of laminar probe depth

The tips of laminar implants were stained before surgery with the orange-red fluorescent membrane stain DiI® (1,1'-Dioctadecyl-3,3,3',3'-Tetramethylindocarbocyanine Perchlorate; Thermo Fisher Scientific, Waltham, MA, USA) for later histological assessment of the electrode position. After completion of the experiments, microlesions of selected channels on the laminar probe were performed under terminal anaesthesia using the electroplating device

NanoZ™ (White Matter LLC, Seattle, WA, USA) applying 10mA direct current for 25 seconds to each respective channel. Immediately following microlesioning, mice were perfused with 0.9 % phosphate buffered saline followed by 4 % paraformaldehyde for tissue preservation. Vibrating microtome (Leica VT1000S) sectioning was used to acquire 50 µm coronal brain slices. Fluorescent staining was performed with 4′,6-diamidino-2-phenylindole (DAPI). After fluorescence microscopy, implantation sites were mapped using a mouse brain atlas[42] and the depth of the laminar implant was assessed measuring the distance between cortical surface and the electrical current induced tissue microlesions.

Ethical approval

All experiments were performed in accordance with the United Kingdom Animal Scientific Procedures Act 1986 under personal and project licences granted by the United Kingdom Home Office. Ethical approval was provided by the Ethical Review Panel at the University of Oxford. Animal holding and experimentation were located at the Biomedical Sciences Building (BSB) and the Behavioural Neuroscience Unit (BNU), University of Oxford.

Bibliography

1. Economo, C. V. Sleep as a problem of localization. *J. Nerv. Ment. Dis.* **71**, 249–259 (1930).
2. Nauta, W. J. H. HYPOTHALAMIC REGULATION OF SLEEP IN RATS. AN EXPERIMENTAL STUDY. *J. Neurophysiol.* **9**, 285–316 (1946).
3. Saper, C. B. & Fuller, P. M. Wake–sleep circuitry: an overview. *Curr. Opin. Neurobiol.* **44**, 186–192 (2017).
4. Liu, D. & Dan, Y. A Motor Theory of Sleep-Wake Control: Arousal-Action Circuit. *Annu. Rev. Neurosci.* (2019). doi:10.1146/annurev-neuro-080317-061813
5. Adamantidis, A. R., Gutierrez Herrera, C. & Gent, T. C. Oscillating circuitries in the sleeping brain. *Nat. Rev. Neurosci.* (2019). doi:10.1038/s41583-019-0223-4
6. Borbély, A. A. A two process model of sleep regulation. *Hum. Neurobiol.* **1**, 195–204 (1982).
7. Vyazovskiy, V. V. *et al.* Cortical Firing and Sleep Homeostasis. *Neuron* **63**, 865–878 (2009).
8. Vyazovskiy, V. V. & Harris, K. D. Sleep and the single neuron: the role of global slow oscillations in individual cell rest. *Nat. Rev. Neurosci.* **14**, 443–451 (2013).
9. Tononi, G. & Cirelli, C. Sleep and the Price of Plasticity: From Synaptic and Cellular Homeostasis to Memory Consolidation and Integration. *Neuron* **81**, 12–34 (2014).
10. Huber, R., Felice Ghilardi, M., Massimini, M. & Tononi, G. Local sleep and learning. *Nature* **430**, 78–81 (2004).
11. Vyazovskiy, V. V. *et al.* Local sleep in awake rats. *Nature* **472**, 443–7 (2011).
12. Krueger, J. M., Nguyen, J. T., Dykstra-Aiello, C. J. & Taishi, P. Local sleep. *Sleep Med. Rev.* **43**, 14–21 (2019).
13. Sanchez-Vives, M. V & Mattia, M. Slow wave activity as the default mode of the cerebral cortex. *Arch Ital Biol* **152**, 147–155 (2014).
14. González-Rueda, A., Pedrosa, V., Feord, R. C., Clopath, C. & Paulsen, O. Activity-Dependent Downscaling of Subthreshold Synaptic Inputs during Slow-Wave-Sleep-like Activity In Vivo. *Neuron* 1–9 (2018). doi:10.1016/j.neuron.2018.01.047
15. Lemieux, M., Chen, J.-Y., Lonjers, P., Bazhenov, M. & Timofeev, I. The Impact of Cortical Deafferentation on the Neocortical Slow Oscillation. *J. Neurosci.* **34**, 5689 LP – 5703 (2014).

16. Saberi-Moghadam, S., Simi, A., Setareh, H., Mikhail, C. & Tafti, M. In vitro Cortical Network Firing is Homeostatically Regulated: A Model for Sleep Regulation. *Sci. Rep.* **8**, 6297 (2018).
17. Neske, G. T. The Slow Oscillation in Cortical and Thalamic Networks: Mechanisms and Functions. *Front. Neural Circuits* **9**, 88 (2016).
18. van Aerde, K. I., Qi, G. & Feldmeyer, D. Cell Type-Specific Effects of Adenosine on Cortical Neurons. *Cereb. Cortex* **25**, 772–787 (2015).
19. Lőrincz, M. L. *et al.* A distinct class of slow (~0.2-2 Hz) intrinsically bursting layer 5 pyramidal neurons determines UP/DOWN state dynamics in the neocortex. *J. Neurosci.* **35**, 5442–58 (2015).
20. Beltramo, R. *et al.* Layer-specific excitatory circuits differentially control recurrent network dynamics in the neocortex. *Nat. Neurosci.* **16**, 227–234 (2013).
21. Chauvette, S., Volgushev, M. & Timofeev, I. Origin of Active States in Local Neocortical Networks during Slow Sleep Oscillation. *Cereb. Cortex* **20**, 2660–2674 (2010).
22. Sanchez-Vives, M. V & McCormick, D. A. Cellular and network mechanisms of rhytmic recurrent activity in neocortex. *Nat. Neurosci.* **3**, 1027–1034 (2000).
23. Sakata, S. & Harris, K. D. Laminar Structure of Spontaneous and Sensory-Evoked Population Activity in Auditory Cortex. *Neuron* **64**, 404–418 (2009).
24. Funk, C. M., Honjoh, S., Rodriguez, A. V., Cirelli, C. & Tononi, G. Local slow waves in superficial layers of primary cortical areas during REM sleep. *Curr. Biol.* **26**, 396–403 (2016).
25. Hoerder-Suabedissen, A. *et al.* Cell-Specific Loss of SNAP25 from Cortical Projection Neurons Allows Normal Development but Causes Subsequent Neurodegeneration. *Cereb. Cortex* (2018). doi:10.1093/cercor/bhy127
26. Gerfen, C. R., Paletzki, R. & Heintz, N. GENSAT BAC cre-recombinase driver lines to study the functional organization of cerebral cortical and basal ganglia circuits. *Neuron* **80**, 1368–1383 (2013).
27. Washbourne, P. *et al.* Genetic ablation of the t-SNARE SNAP-25 distinguishes mechanisms of neuroexocytosis. *Nat. Neurosci.* **5**, 19–26 (2002).
28. Buzsáki, G. Theta Oscillations in the Hippocampus. *Neuron* **33**, 325–340 (2002).
29. Boyce, R., Glasgow, S. D., Williams, S. & Adamantidis, A. Causal evidence for the role of REM sleep theta rhythm in contextual memory consolidation. *Science (80-.).* **352**, 812 LP – 816 (2016).

30. Huber, R., Deboer, T. & Tobler, I. Effects of sleep deprivation on sleep and sleep EEG in three mouse strains: empirical data and simulations. *Brain Res.* **857**, 8–19 (2000).
31. Vyazovskiy, V. V, Ruijgrok, G., Deboer, T. & Tobler, I. Running Wheel Accessibility Affects the Regional Electroencephalogram during Sleep in Mice. *Cereb. Cortex* **16**, 328–336 (2005).
32. Huber, R., Deboer, T. & Tobler, I. Topography of EEG Dynamics After Sleep Deprivation in Mice. *J. Neurophysiol.* **84**, 1888–1893 (2000).
33. Franken, P., Dijk, D. J., Tobler, I. & Borbely, A. A. Sleep deprivation in rats: effects on EEG power spectra, vigilance states, and cortical temperature. *Am. J. Physiol. Integr. Comp. Physiol.* **261**, R198–R208 (1991).
34. Morairty, S. R. *et al.* A role for cortical nNOS/NK1 neurons in coupling homeostatic sleep drive to EEG slow wave activity. *Proc Natl Acad Sci U S A* **110**, 20272–20277 (2013).
35. Frank, M. G. & Heller, H. C. The Function(s) of Sleep. in *Sleep-Wake Neurobiology and Pharmacology* (eds. Landolt, H.-P. & Dijk, D.-J.) 3–34 (Springer International Publishing, 2019). doi:10.1007/164_2018_140
36. Brüning, F. *et al.* Sleep-wake cycles drive daily dynamics of synaptic phosphorylation. *Science (80-.).* **366**, eaav3617 (2019).
37. Honda, T. *et al.* A single phosphorylation site of SIK3 regulates daily sleep amounts and sleep need in mice. *Proc. Natl. Acad. Sci.* **115**, 10458 LP – 10463 (2018).
38. Williams, J. A. & Naidoo, N. Sleep and cellular stress. *Curr. Opin. Physiol.* **15**, 104–110 (2020).
39. Kempf, A., Song, S. M., Talbot, C. B. & Miesenböck, G. A potassium channel β-subunit couples mitochondrial electron transport to sleep. *Nature* 1 (2019).
40. Eichenbaum, H. On the Integration of Space, Time, and Memory. *Neuron* **95**, 1007–1018 (2017).
41. McKillop, L. E. *et al.* Effects of Aging on Cortical Neural Dynamics and Local Sleep Homeostasis in Mice. *J. Neurosci.* **38**, 3911 LP – 3928 (2018).
42. Paxinos, G. & Franklin, K. B. J. *Paxinos and Franklin's the mouse brain in stereotaxic coordinates*. (Elsevier Academic Press, 2019).

Acknowledgements

We thank Thomas Jahans-Price and Xudong Wang for their help with establishing the microlesion protocol; Merima Sabanovic, Vincent van der Vinne and Laura McKillop for their advice on statistics and figure production; Kristina Parley for her support in the histological procedures. Stuart Peirson for his advice on the experimental design. This work was supported by the Wellcome Trust PhD studentship 203971/Z/16/Z, Wellcome Trust Strategic Award 098461/Z/12/Z, John Fell OUP Research Fund Grant 131/032, and Medical Research Council (UK) grant MR/N026039/1.

Author contributions

ZM and VVV initiated and proposed the study with pilot experiments done by TY. LBK, TY, CJA, AHS, ZM, and VVV designed the experiments. LBK, TY, MCCG, and CBD conducted the experiments on the transgenic mouse model. LBK, CBD, and MCK conducted the experiments on wild type mice. LBK, MCK, and AHS performed the histology. AHS and ZM developed, validated, and provided the transgenic mice. LBK and VVV analysed the data. LBK and VVV wrote the manuscript. All of the authors discussed the results and commented on the manuscript.

Competing interests

The authors declare no competing interests.

Figures

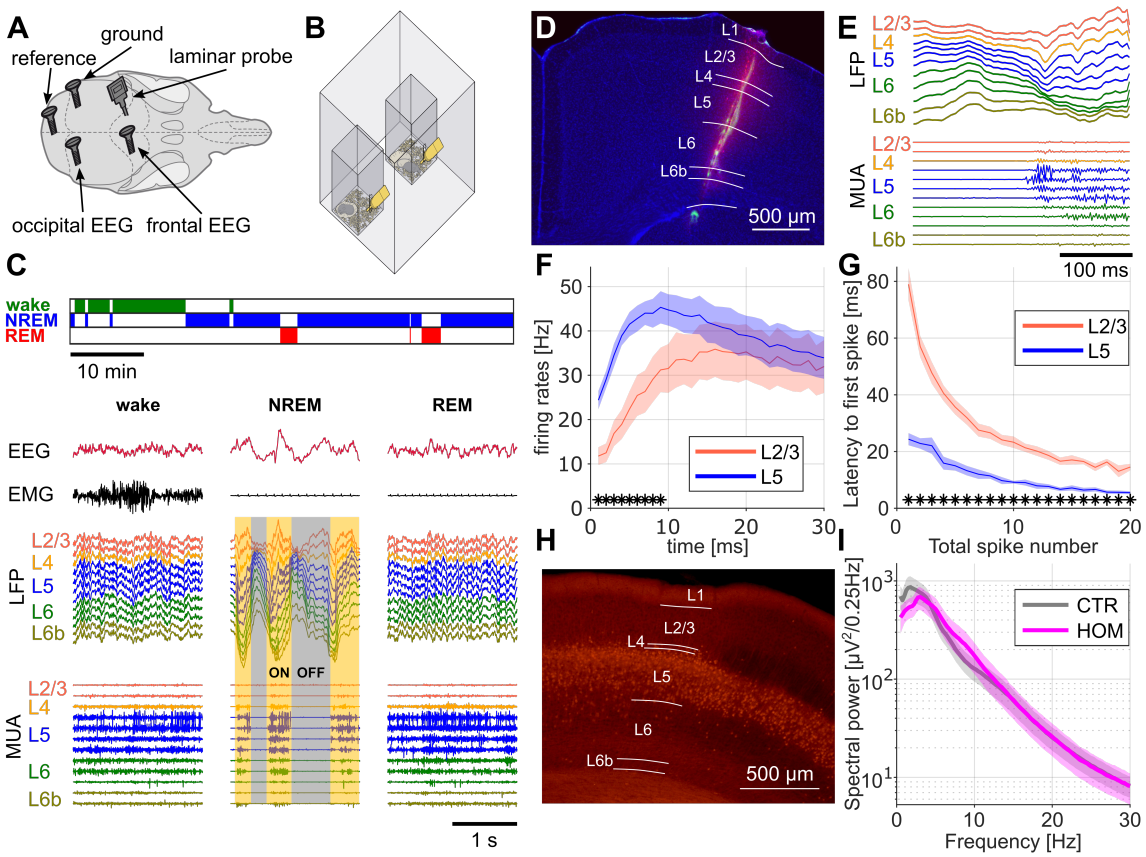

Figure 1: Cortical recordings in freely moving mice implicate layer 5 in sleep
A) Schematic of electrode positions in relation to the skull. Mice were implanted with EEG screws over the right frontal and occipital cortex referenced against a cerebellar screw. A laminar probe is located in the left primary motor cortex, grounded to a left occipital screw and referenced against a cerebellar screw. EMG electrodes on the neck muscles are not depicted in the diagram. B) Recording conditions: Mice were individually housed under a 12h:12h light-dark cycle in plexiglas cages placed inside a Faraday chamber with free access to food and water C) Hypnogram colour coded for the three vigilance states wake, NREM, and REM sleep, as well as EEG, EMG, LFP, and MUA traces showing characteristic signatures of the respective vigilance states. In the example traces from NREM sleep, ON periods with neuronal firing and depth-negative slow waves as well as OFF periods marked by neuronal silence and depth-positive slow waves are highlighted with transparent yellow and grey panels, respectively. D) Histological determination of the location of the laminar implant. The DiI trace (red) indicates the electrode tract while fine electrode marks (green) in a distance of 100 µm between individual channels verify the exact depth of several individual channels on a DAPI counterstained (blue) coronal section. E) Example of one representative OFF-ON transition. Note that population activity starts in layer 5. F) Firing rates at the beginning of OFF-ON transitions. Note that layer 5 presents an earlier surge in firing rate over the first 9 ms after the OFF-ON transition while firing rates are not significantly different between 10 and 30 ms (two-tailed paired t-test for each 1ms time bin). G) Latency to the first spike for matched spike numbers during the first 200 ms of the ON period. For any given total spike count analysed (1 to 20 counts), layer 5 has a shorter latency to the first spike than layer 2/3 (two-tailed paired t-

test for each total spike number) H) Example of Cre-expression under the Rbp4-Cre promotor using the tdTomato indicator Ai14. Note that Cre-positive cells in isocortex are largely restricted to layer 5. K) Frontal EEG spectra of homozygous cortical SNAP25-ablated (HOM) and control animals (CTR). Note that for none of the frequency bins a statistical difference was observed between HOM and CTR mice (two-tailed t-tests for independent samples performed on log-transformed spectra, significance threshold of p=0.05, no correction for multiple comparison.
N=7 for laminar analysis in WT animals (panels F,G). N=5 (CTR) and n=8 (HOM) for absolute EEG spectra of the cortical SNAP25-ablated mouse model (panel I).
DiI: 1,1'-Dioctadecyl-3,3,3',3'-Tetramethylindocarbocyanine Perchlorate. EEG: electroencephalogram. EMG: Electromyogram. LFP: Local field potentials. MUA: Multi unit activity. NREM: Non-rapid eye movement sleep. REM: Rapid eye movement sleep. CTR: control animals. HOM: homozygous animals.

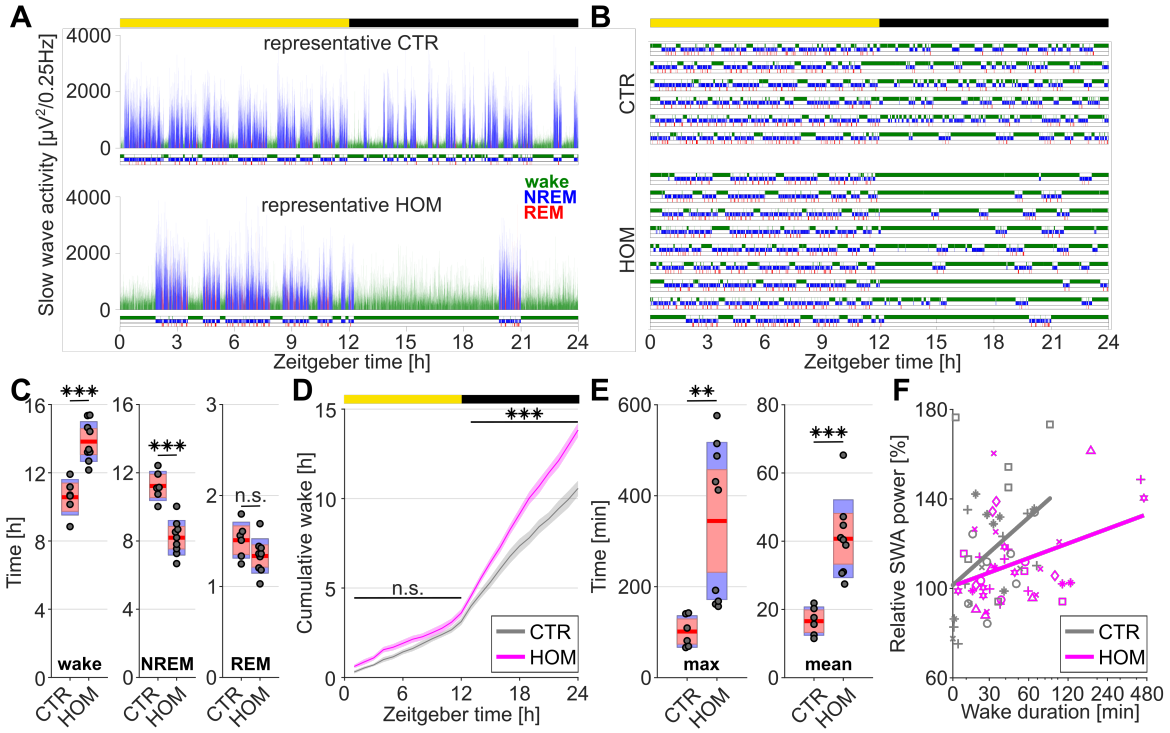

Figure 2: Selective cortical SNAP25-ablation alters sleep architecture
A) Hypnograms and EEG slow wave activity (SWA, spectral power between 0.5 and 4.0 Hz) for each 4 s epoch of one representative animal from each genotype in undisturbed 24 h baseline recordings. B) Hypnograms from all individual control (CTR) and cortical SNAP25-ablated (HOM) animals under undisturbed baseline conditions. Note the increased amount of wakefulness and long wake episodes in HOMs. Vigilance states in A&B colour coded: wake=green, NREM=blue, REM=red. C) Amount of time spent in wake, NREM, and REM during undisturbed 24 h baseline recordings. Note that HOMs spent 3 h and 16 min more time awake compared to CTRs. D) Cumulative amount of wakefulness. Note that the slope of wake accumulation is similar between genotypes during the light period but steeper for HOMs compared to CTRs during the dark period (ZT 12-24)(mixed ANOVA with within-subject factor 'LightDarkPeriod' and between-subject factor 'genotype'. Positive interaction for 'LightDarkPeriod' and 'genotype': $F(1,13)=39.96$, $p<0.001$. Post-hoc two-tailed t-tests for independent samples: Light Period: $t(13)=-1.62$, $p=0.13$; Dark Period: $t(13)=-7.07$, $p < 0.001$). E) Maximum and mean duration of individual wake episodes over 42 hours (BL and SD day excluding the 6 h sleep deprivation period). Note that for HOMs both the maximum and mean duration of wake episodes is longer than for CTRs (t-test for independent samples. Significant difference in maximum duration of wake episodes between genotypes: $t(8.94)=-4.11$, $p=0.003$. Significant difference in mean duration of wake episodes between genotypes: $t(13)=-4.94$, $p<0.001$). F) Relationship between wake duration and relative SWA power during NREM epochs compared for 15-minute time windows after vs. before wake episodes of at least 15 minute duration. Note the reduced slope of the relationship between SWA ratio and duration of wake episodes in HOMs (general linear model with 5 factors: mouseID, mouseID x episode duration (random factors), genotype, episode duration, and genotype x episode duration (fixed factors); dependent variable: SWA ratio post/pre sleep; $F(1,57.37)=6.44$, $p=0.014$). Individual animals are represented with different symbols.

Number of animals: n=6 CTR and n=9 HOM for vigilance state analyses (panels C, D, E), n=5 CTR and n=8 HOM for analysis of SWA (panel F). Yellow and black bars above panels A, B, and D indicate light and dark periods, respectively. Panels C and E present grouped data including group mean (red line), 95% confidence interval (pink box), and one standard deviation (blue box) with individual data points overlaid.
EEG: electroencephalogram. NREM: Non-rapid eye movement sleep. REM: Rapid eye movement sleep. CTR: control animals. HOM: homozygous animals. ZT: zeitgeber time. BL: baseline. SD: sleep deprivation.

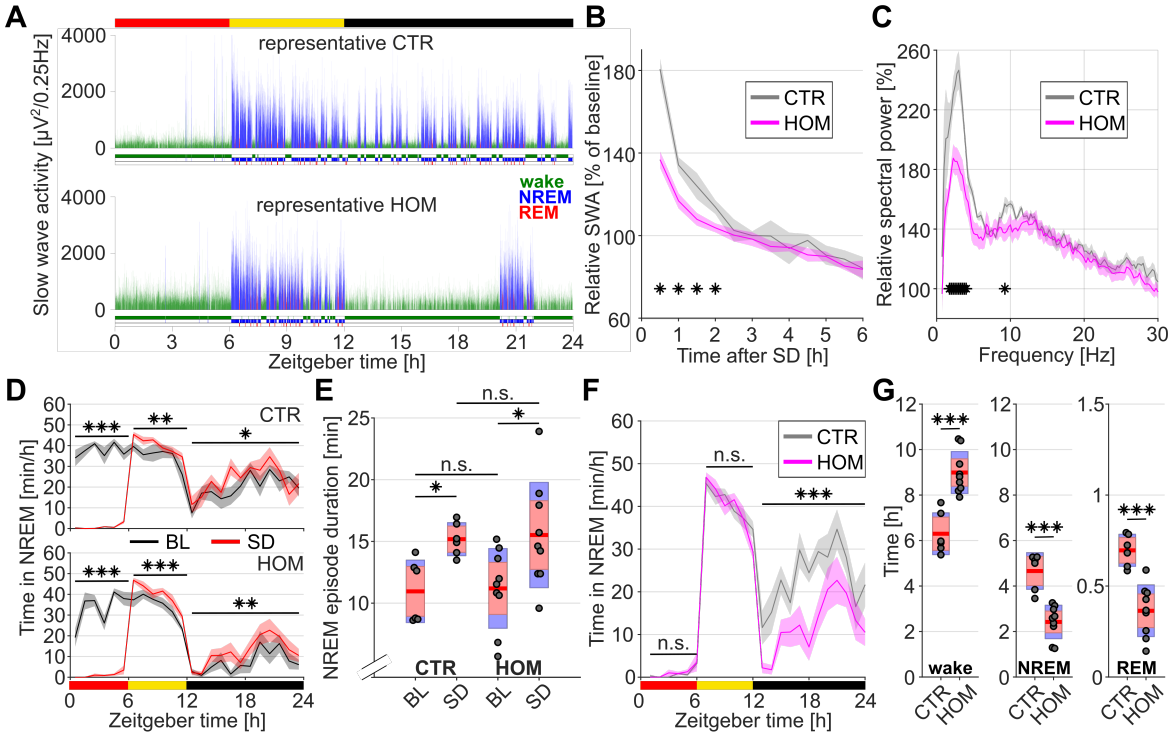

Figure 3: Selective cortical SNAP25-ablation alters homeostatic sleep regulation
A) Hypnograms with EEG slow wave activity (SWA, power between 0.5 and 4.0 Hz) for each 4 s epoch of one representative animal from each genotype in 24 h recordings with 6 h sleep deprivation at light onset (red bar above graph). B) The time course of SWA after sleep deprivation plotted in 30-min intervals. Note that the levels of SWA following sleep deprivation are lower in cortical SNAP25-ablated (HOM) animals during the first 2 hours compared to control (CTR) animals (mixed ANOVA with within-subject factor 'time' and between-subject factor 'genotype'. Significant interaction between 'time' and 'genotype': $F(11,121) = 7.65$, $p < 0.001$. Post-hoc comparison with two-tailed t-tests for independent samples significant for time bins 1-4 (30-120 min)) C) Relative spectral power in NREM sleep during the first hour after sleep deprivation compared with baseline NREM sleep. Note that the characteristic increase in spectral power in low frequencies in response to sleep deprivation is smaller in HOMs compared to CTRs (bin-wise comparison for each frequency bin of 0.25 Hz between 0.5 and 30.0 Hz using two-tailed t-tests for independent samples. Significant frequency bins 7-16 and 37 correspond to the frequency range 1.5 to 3.75 Hz as well as 9 Hz; significance threshold p=0.05; no correction for multiple comparisons applied). D) Time course of NREM sleep for each genotype compared between BL and SD day. Both genotypes show an increase of time in NREM sleep following sleep deprivation (red bar below graph) compared to their individual baselines (repeated measures ANOVAs with within-subject factors 'time' and 'condition'. Main effects: CTR-animals $F(1.10,5.50)=184.84$, $p<0.001$), HOM-animals: $F(2,16)=195.24$, $p<0.001$; post-hoc contrasts analysed with two-tailed t-tests for paired samples. All contrasts significant for $p<0.05$). E) Mean duration of NREM episodes during ZT6-7 on BL and SD days. Note that both genotypes show an increased duration of NREM episodes compared to their own baseline with no difference between genotypes (mixed ANOVA with within-subject factor 'time' and between-subject factor 'genotype'. No main effect for the interaction 'time' and 'genotype' or for between-subject factor 'genotype' but

significant effect for within-subject factor ‘time’: $F(1,13)=13.71$, $p=0.003$; post-hoc contrasts for comparison of time windows in each genotype analysed with two-tailed t-tests for paired samples. Both contrasts significant for $p<0.05$). F) Time course of NREM sleep on a sleep deprivation day compared between genotypes. Note that HOMs and CTRs do not differ in the time spent asleep during sleep deprivation (red bar below graph) or in the initial rebound sleep during the 6h in light conditions after sleep deprivation but HOMs sleep less during the 12 h dark period following sleep deprivation (mixed ANOVA with within-subject factor ‘time’ and between-subject factor ‘genotype’. Main effect for interaction between ‘time’ and ‘genotype’: $F(1.16,15.01)=30.93$, $p<0.001$; post-hoc contrasts for comparison of genotypes at each time interval not significant during SD or during remainder of light period after SD but for dark period; significance threshold of $p=0.05$). G) Amount of time spent in wake, NREM, and REM during 12 h dark period following sleep deprivation. Note that HOMs spent more time awake and less asleep compared to CTRs (Mann-Whitney U test applied as assumption of normality violated, $p<0.001$ for all vigilance states).
N=6 CTR and n=9 HOM for vigilance state analyses (panels D, E, F, G), n=5 CTR and n=8 HOM for analysis of SWA and EEG spectra (panel B,C). Red, yellow and black bars above panels A, D, and F indicate sleep deprivation, light and dark periods, respectively. Panels E and G present grouped data including group mean (red line), 95% confidence interval (pink box), and one standard deviation (blue box) with individual data points overlaid.
EEG: electroencephalogram. NREM: Non-rapid eye movement sleep. REM: Rapid eye movement sleep. CTR: control animals. HOM: homozygous animals. ZT: zeitgeber time. BL: baseline. SD: sleep deprivation.

Supplementary figures

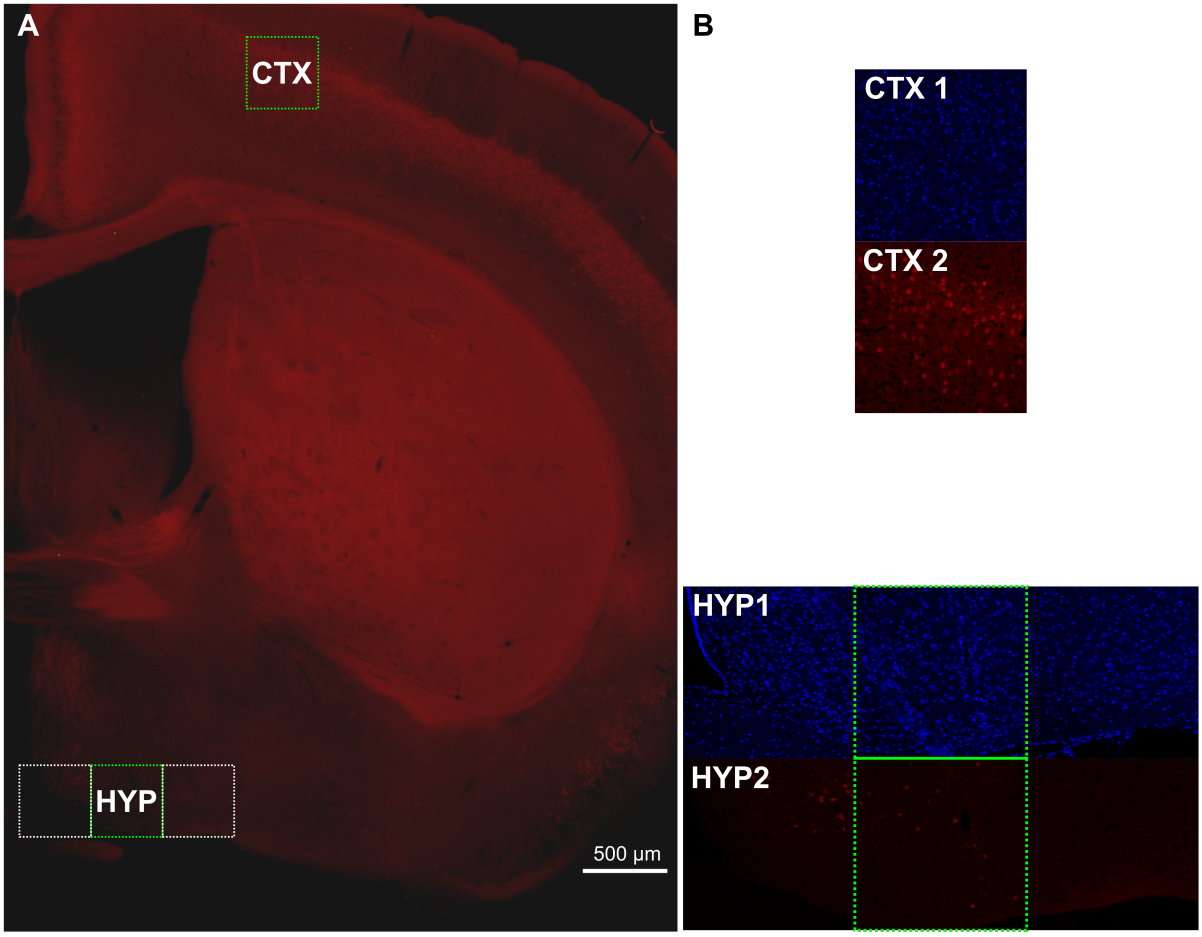

Suppl. Figure 1: Comparison of Cre-expression in the Rbp4-Cre mouse line between cortical layer 5 and a hypothalamus

A) Coronal section of a Rbp4-Cre;Ai14;Snap25$^{fl/+}$ mouse brain (anterior-posterior position: approximately Bregma ±0.0 mm) indicating areas, which were further examined for Cre-expression using confocal imaging of DAPI stained slices. For the hypothalamic area three neighbouring confocal tiles (425x425 µm each) were acquired starting from the lateral surface of the third ventricle. Cells were counted in the green highlighted rectangles of equal size. B) DAPI stained confocal images from cortex (CTX) and hypothalamus (HYP) in the blue fluorescence channel used for cell counting (CTX1 and HYP1) and in the red fluorescence channel (CTX2 and HYP2) used to identify Cre-expression in the respective cells indicated by expression of the red fluorescent STOP-floxed tdTomato reporter Ai14. Cell counts on corresponding coronal sections in three brains revealed that 20.53±0.98% (480 of 2342 counted) of cortical cells were tdTomato positive, while only 1.15±0.40% (35 of 3006 counted) of hypothalamic cells expressed the red fluorescent indicator.

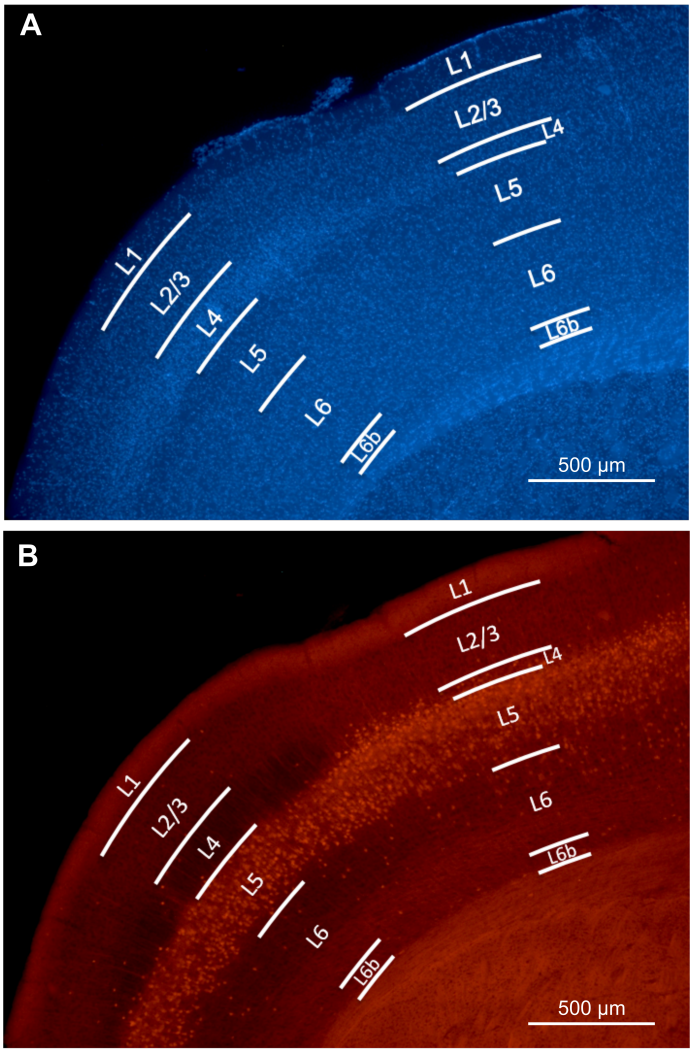

Suppl. Figure 2: Identification of cortical layers in a representative coronal brain slice covering primary motor and sensory cortex

A) Cortical layers were determined using DAPI staining and identification of characteristic anatomical features of specific layers such as cell density and nuclear size. B) Image shows the largely restricted expression of the red fluorescent protein tdTomato in layer 5 in both primary motor and sensory cortex. The selective Cre-expression was driven by Rbp4 promoter that cleaved the STOP-floxed site in the tdTomato reporter Ai14 mouse. Anterior-posterior position: approximately Bregma ±0.75 mm.

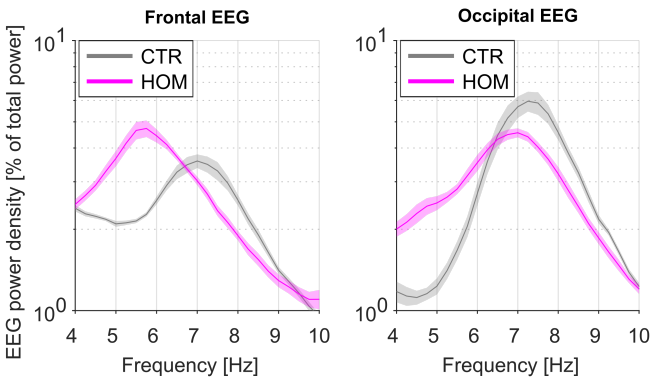

Suppl. Figure 3: Relative spectral power in the theta frequency range during REM sleep in homozygous (HOM) Rbp4-Cre;Ai14;Snap25$^{fl/fl}$ mice compared to Cre-negative littermates (CTR). Note that the peak of theta activity is shifted towards lower frequencies in HOMs (n=8) compared to CTRs (n=5) in both the frontal (HOM: 6.09±0.07 Hz; CTR: 6.95±0.09 Hz; p=0.002, Mann-Whitney U test) and occipital (HOM: 6.91±0.10 Hz; CTR: 7.35±0.06 Hz; p=0.015, Mann-Whitney U test) EEG derivation.

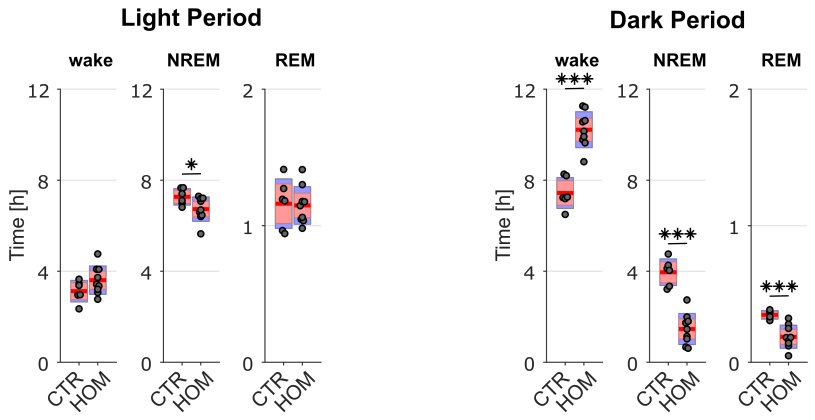

Suppl. Figure 4: Amount of time spent in wake, NREM, and REM during the light period and dark period of undisturbed baseline recordings

During the light period, the distribution between vigilance states is similar between genotypes (wake: 3.13±0.19 h (CTR) vs. 3.61±0.21 h (HOM), t(13)=-1.62, p=0.130; NREM: 7.27±0.15 h (CTR) vs. 6.73±0.18 h (HOM), t(13)=2.17, p=0.049; REM: 1.16±0.07 h (CTR) vs. 1.15±0.05 h (HOM), t(13)=0.149, p=0.884), while strong differences occur during the dark period (wake: 7.44±0.28 h (CTR) vs. 10.22±0.26 h (HOM), t(13)=-7.07, p<0.001; NREM: 3.96±0.24 h (CTR) vs. 1.46±0.23 h (HOM), t(13)=7.32, p<0.001; REM: 0.35±0.01 h (CTR) vs. 0.19±0.03 h (HOM), t(13)=4.43, p=0.001). N=6 CTR and n=9 HOM. Data is presented as group mean (red line), 95% confidence interval (pink box), and one standard deviation (blue box) with individual data points overlaid.

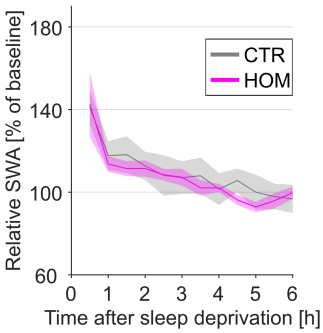

Suppl. Figure 5: Time course of NREM slow wave activity (SWA) after sleep deprivation in the occipital EEG derivation

Slow wave activity (SWA) during NREM sleep is plotted in 30-min intervals for a 6 h time window after sleep deprivation for the occipital derivation. No significant differences between genotypes were observed (mixed ANOVA with within-subject factor 'time' and between-subject factor 'genotype'. Interaction between 'time' and 'genotype': $F(1.907,20.975) = 0.301$, $p = 0.73$. Post-hoc comparison with two-tailed t-tests for independent samples reveals no significant differences for any of the 12 time bins. Significance threshold of $p=0.05$; no correction for multiple comparisons applied). N=5 CTR and n=8 HOM.